Photosynthetic Bacterial Light-Harvesting Antenna Complexes Adsorbed on Silica Nanoparticles Revealed by Silica Shell-Isolated Au Nanoparticle-Enhanced Raman Spectroscopy

ARTICLE *in* THE JOURNAL OF PHYSICAL CHEMISTRY C · MARCH 2012

Impact Factor: 4.77 · DOI: 10.1021/jp211841a

4 AUTHORS:

Lu-Chao Du
Chinese Academy of Sciences
8 PUBLICATIONS **118** CITATIONS
SEE PROFILE

Yi-Fan Huang
Leiden University
30 PUBLICATIONS **845** CITATIONS
SEE PROFILE

Bin Ren
Xiamen University
273 PUBLICATIONS **8,657** CITATIONS
SEE PROFILE

Yu-Xiang Weng
Chinese Academy of Sciences
45 PUBLICATIONS **781** CITATIONS
SEE PROFILE

THE JOURNAL OF PHYSICAL CHEMISTRY C

Article

pubs.acs.org/JPCC

Photosynthetic Bacterial Light-Harvesting Antenna Complexes Adsorbed on Silica Nanoparticles Revealed by Silica Shell-Isolated Au Nanoparticle-Enhanced Raman Spectroscopy

Lu-Chao Du,[†] Yi-Fan Huang,[‡] Bin Ren,[‡] and Yu-Xiang Weng*[,†]

[†]Laboratory of Soft Matter Physics, Institute of Physics, Beijing 100190, China

[‡]State Key Laboratory of Physical Chemistry of Solid Surfaces and Department of Chemistry, College of Chemistry and Chemical Engineering, Xiamen University, Xiamen 361005, Fujian, China

ABSTRACT: Assembling of photosynthetic light-harvesting proteins with inorganic nanoparticles can be a promising strategy for developing artificial solar cells. However, characterization of protein adsorption and its spatial orientation with respect to the interface is still a challenging task. Here we report surface-enhanced Raman spectra of light-harvesting antenna complexes (LH2) from two different photosynthetic bacteria adsorbed onto Au core silica shell ($Au@SiO_2$) nanoparticles to illustrate LH2 adsorption and orientation at the interface. The surface plasmon enhanced Raman spectra of typical vibrational modes of carotenoids are used as the intrinsic reporter of LH2 adsorbed on $Au@SiO_2$. Carotenoid molecules are asymmetrically located inside the disk-like LH2 closest to cytoplasmic side, leading to an orientation-dependent surface-enhanced Raman gain when the LH2 binds to the interface with one of its two end surfaces. We find that the Raman gain factors for LH2 from *Rba. sphaeroides* are larger than those from *Rps. acidophila*, suggesting that these two different LH2s adsorbed on the negatively charged silica shell with opposite orientation of their end surfaces carrying opposite charges. This is further supported by the observed difference in the B850 excited-state lifetime change for these two different LH2s when adsorbed onto silica nanoparticles, where the lifetime of B850 acts as an intrinsic reporter for nanoparticle-induced protein deformation which is also orientation-dependent, owing to the asymmetrical location of B850 ring inside the LH2.

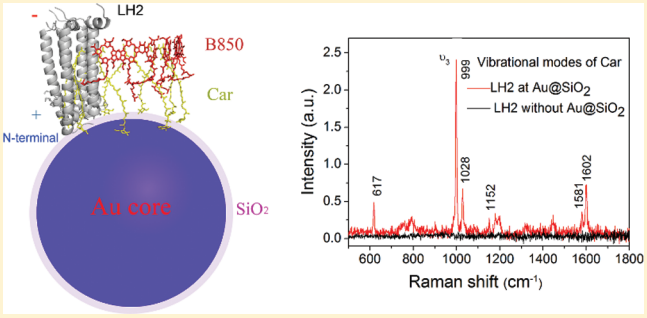

INTRODUCTION

With the advent of nanotechnology in biology and medicine, the need for conjugation of nanoparticles (NPs) to proteins has grown constantly. Attachment of proteins to NPs forming a new kind of materials known as inorganic−protein hybrid has found its application in many areas, such as imaging, implant materials, catalysis, biosensors, and drug delivery in a biological science.[1,2] This hybrid material has also been used in energy research. It has been reported that binding of quantum dots acting as light-harvesting antenna to the reaction center (RC) of the photosynthetic bacteria can significantly increase the light conversion efficiency of RC, providing an example of inorganic−protein hybrid materials for artificial photovoltaic systems.[3] Other authors have shown that the stability of the photosynthetic membrane proteins has been increased when incorporated into silica nanopores, while their activities of light absorption, excitation energy transfer, and charge separation were preserved.[4,5]

The elemental step of conjugating proteins to NPs involves adsorption or binding of proteins onto an inorganic interface. Therefore it is imperative to know that whether the proteins have ever been conjugated onto the NPs and how proteins are bounded to the interface as well as their spatial orientation with respect to the interface, since the function of the protein can be closely related to the orientation, e.g., the charge transfer pathway within the RC is vectorial guided by a series of donors and acceptors located on the path.[3] A number of methods, based on different principles such as optical absorption, refractive index changes, radio labeling, electrochemical microbalances, fluorescence marker, neutron reflection etc., have been developed toward this purpose.[6,7] However, owing to the demand of high interfacial as well as molecular structural sensitivity for the detection techniques, development of a sensitive method for detecting the interfacial binding and orientation of the adsorbed proteins at the hybrid interface is still a challenging task.

Recently, Li et al. reported a new technique of surface-enhanced Raman spectroscopy named shell-isolated nanoparticle-enhanced Raman spectroscopy (SHINERS).[8] The essence of this method is to coat the Raman signal amplifier, i.e., Au nanoparticles, with a spread monolayer of silica or alumina, which was then used to detect the Raman signal of the sample in the vicinity of the core−shell nanoparticles. The shell has a dual role: it can prevent NP agglomeration and avoid the direct interaction of protein with the metal surface, overcoming the problem of protein denaturation.

Received: December 8, 2011
Revised: February 22, 2012
Published: March 6, 2012

In this way, the Raman signal can be substantially enhanced due to a large number of Au NPs, which gives a possibility of detecting the interfacial binding or protein adsorption at the shell layer.

In our previous work, we assembled light-harvesting antenna complex LH2 from photosynthetic bacteria to silica NPs to investigate LH2 protein deformation on the silica NPs and used the excited-state lifetime of B850 bacteriochlorophyll (BChl) aggregate ring in LH2 as an intrinsic probe for the LH2 protein deformation. It is believed that self-assembling of LH2 onto the silica NP is realized through electrostatic interaction between the positively charged end face of the LH2 protein and the negatively charged silica sphere. However, the orientation of the LH2 (either cytoplasmic or periplasmic side) on the surface of silica NPs remains to be determined experimentally.[9] In the current work, we employ SHINERS as a novel method for investigation of the interfacial binding and molecular orientation of LH2 adsorbed on silica NPs, where the silica shell on the Au NP is used not only for preventing the agglomeration of Au NPs, but also as the interfacial material onto which the proteins are adsorbed. Furthermore, during the coating process, the silica shell will remove the impurities staying on the surface of the Au core to minimize the background.

EXPERIMENTAL SECTION

LH2s from strain *Rhodobacter* (*Rba.*) *sphaeriodes* and *Rhodopseudomonas* (*Rps.*) *acidophila* were prepared. The culture of the cells which followed the reported protocols[10] and the preparation and purification of LH2 complexes, as well as the assembling of LH2 onto the NPs, have been described elsewhere.[9] The Au@SiO_2 core−shell NPs were prepared by wet chemical synthesis method according to the literature (see ref 8 and the supporting information therein). Briefly, an aliquot of 1.4 mL 1% sodium citrate solution (mass fraction) was added to 200 mL 0.01% boiling $HAuCl_4$ solution. Under vigorous stirring, the mixture was refluxed for 1 h, and this Au NP solution was used for SiO_2 deposition. Then 400 μL of 1 mM (3-aminopropyl) trimethoxysilane (APTMS) solution was added to 30 mL of as-prepared Au NP solution, and the mixture was stirred for 15 min at room temperature followed by an addition of 3 mL 0.54% sodium silicate solution with a pH ranging from 9.5 to 10.5. Finally, the solution was immersed in boiling water for 1 h under vigorous stirring. The size of the Au NPs and the thickness of the silica layer were examined by a JEM 2010 transmission electron microscope (TEM) from JEOL (Peabody, MA). Silica colloidal solutions were commercially available from different sources: Alfa Chem (New York, USA); EKA Chemicals (Bohus, Sweden), and Technical Institute of Physics and Chemistry, CAS (Beijing, China). Their average sizes were evaluated statistically from the TEM images.

The Raman spectra were recorded in a back scattering geometry. The samples were excited by laser at a power of 0.9 mW focused through a 50× objective lens, resulting in a spot size around 1−2 μm in diameter. The spectral resolution of the Raman spectrometer was 1.0 cm^{-1}. For the resonant Raman scattering experiment, a HR800 micro-Raman spectrometer (Horiba Jobin Yvon, France) was used, and the excitation source was a solid-state laser with an output wavelength of 532 nm. For nonresonant excitation, a 632.8 nm He−Ne laser and a Reinshaw spectrometer (Gloucestershire, UK) were used. The fluorescence lifetimes were measured on an Edinburgh NF900 time-resolved fluorometer (Edinburgh Instruments, Livingston, UK).

The LH2−Au@SiO_2 solutions (70 g/mL) were prepared at varied pH ranging from 3.7 to 9.5. The concentration of LH2 was adjusted to $OD_{850nm} \approx 1.0$ cm^{-1} in 20 mM Tris-HCl buffer (pH = 8) containing 0.1% LDAO. LH2 was mixed with Au@SiO_2 solution and kept stirring about 30 min under Ar gas protection, then kept in the dark at 4 °C for at least 24 h. The isoelectric point of silica NP is 3,[11] with a zeta potential ranging from −50 to −100 mV at a pH between 3 and 11,[12] thus its surface is negatively charged under the LH2 adsorption condition.

RESULTS AND DISCUSSION

Figure 1 shows a typical TEM image of Au@silica NP with an averaged Au core size about 60 nm and a silica shell about 5 nm in thickness. Figure 2 displays the plasmonic band absorption spectrum of the corresponding Au@silica NP solution, together with UV−visible absorption spectrum of the LH2 solution. The arrows indicate the resonant and the nonresonant Raman excitation wavelengths used in the experiment respectively.

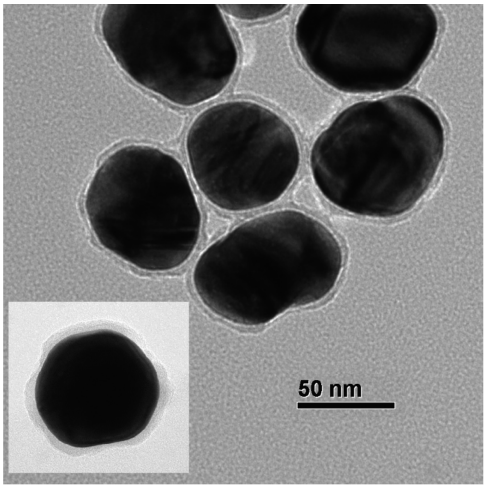

Figure 1. TEM images of Au@SiO_2 NPs. The size of Au core is about 60 nm in diameter. The mainframe is the image of Au@SiO_2 NPs for adsorption of LH2 from *Rps. acidophila*, the shell thickness is about 4 nm. The image at the left corner is that for adsorption of LH2 from *Rba. sphaeroides,* the shell thickness is about 5 nm.

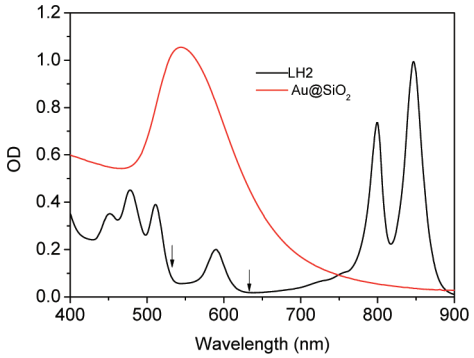

Figure 2. UV−visible absorption spectrum of Au@SiO_2 NP solution (red line) and solution of LH2 from *Rba. sphaeroides* (black line), respectively. The two arrows indicate the Raman excitation wavelengths.

Carotenoid (Car) molecules generally yield very intense resonance Raman (RR) signals, which are dominated by four

dx.doi.org/10.1021/jp211841a | J. Phys. Chem. C 2012, 116, 6993−6999

regions of relatively high intensity bands at approximately 950, 1010, 1160, and 1520 cm^{-1}. These bands have been attributed to out-of-plane C—H modes (ν_4 modes), the stretching modes of C—CH_3 bonds between the main chain and side methyl carbons (ν_3 modes), C—C bond stretching modes mixed with C—H bond bending modes (ν_2 modes), and the stretching modes of conjugated C═C bonds (ν_1 modes).[13] These typical spectroscopic features have been extensively used for probing the structure and geometry of Car molecules with an all-trans configuration in photosynthetic light-harvesting and a cis configuration in RC complexes.[14,15]

We selected two Raman excitation wavelengths, i.e., 532 and 632.8 nm to acquire the surface-enhanced Raman spectra of LH2 from *Rba. sphaeroides* adsorbed on Au@SiO_2 NPs, where the excitation wavelength at 532 nm is not only in resonance with the Car absorption band, but also with the plasmonic absorption of the core−shell Au NPs. While that at 632.8 nm is not in resonance with the absorption band of Car molecules but with that of the core−shell Au NPs. Figure 3a compares plasmonic core−shell Au NP-enhanced RR and normal RR spectra of LH2 (*Rba. sphaeriodes*; after subtraction of the fluorescence background) in the vibrational frequency region of Car excited at 532 nm; Figure 3b compares the plasmonic core−shell Au NP-enhanced Raman and the normal Raman spectra of the same sample excited at 632.8 nm. In Figure 3a plasmonic core−shell Au NP-enhanced RR spectrum is almost an amplified RR spectrum but with a varied gain factor between 2.0 to 3.5 for the different vibrational modes when the corresponding RR intensity of free LH2 solution at pH = 8.0 is used as the scaling reference. The varied surface-enhanced Raman gain factor is a typical feature of surface plasmon enhanced Raman spectra of Car molecules observed in bacterial photosynthetic membranes of *Rba. sphaeroides* before.[15] In Figure 3b the spontaneous Raman spectrum is too weak to be acquired under this condition, while the plasmonic core−shell Au NP-enhanced Raman signals are still discernible. Figure 3c compares the plasmonic core−shell Au NP-enhanced Raman spectra of Car at resonant and nonresonant excitation. Apparently, the relative peak intensities of these two spectra are quite different, and the plasmonic core−shell Au NP-enhanced Raman spectrum at nonresonant excitation may better reflect the surface selection rule.[16]

We found that The RR spectra of Car molecules in LH2 from *Rba. sphaeroides* and *Rps. acidophila* (data not shown) are quite similar, though Car in the former is sphaeroidene while that in the latter is rhodopsin-glucoside. Figure 4 presents gain factors of surface plasmon enhancement of Car molecules at three different vibrational modes υ_1, υ_2, and υ_3 excited at 532 nm for LH2s from *Rba. sphaeroides* and *Rps. acidophila* respectively, where the corresponding RR intensity of free LH2 solution at pH = 8.0 are used as the scaling reference. The gain factors for the three vibrational modes are plotted against the pH ranging from 3.7 to 9.5, which exhibit a maximum gain value indicating an optimal pH range for assembling of LH2 onto the Au@SiO_2 NPs, i.e., pH = 6−7 for the former and 7−8 for the latter. The difference in the optimal pH range suggests a varied electrostatic property of the contacting end surfaces of these two different LH2 protein complexes. Another significant feature is that the gain factors for the LH2 from *Rps. acidophila* are significantly smaller those of *Rba. sphaeroides*.

To further illustrate the effect of interfacial binding of LH2 onto NPs, we conducted the excited-state lifetime measurement of LH2 adsorbed on silica NPs of varied size at a pH of 8.0.

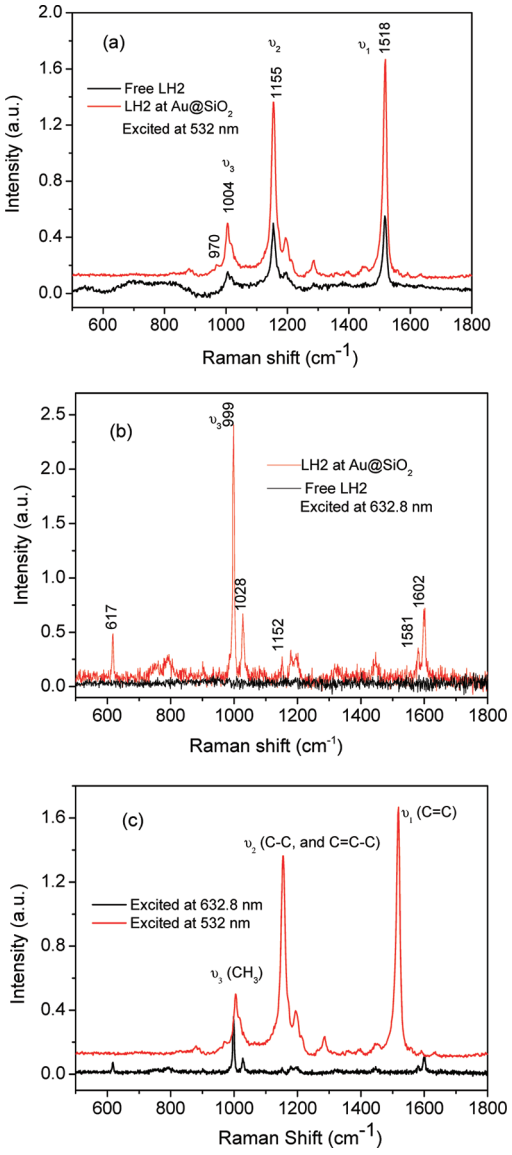

Figure 3. Surface-enhanced Raman spectra of LH2 from *Rba. sphaeroides* adsorbed on Au@SiO_2 NPs acquired at different excitation wavelengths displayed in the vibrational frequency region of Car. (a) Resonant excitation at 532 nm with (in red) and without (in black) Au@SiO_2 NPs at a given pH value of 5.8. (b) Nonresonant excitation at 632.8 nm with (in red) and without (in black) Au@SiO_2 NPs at a given pH value of 8.0. (c) Spectral comparison of resonant (in red) and nonresonant (in black) excitation in presence of Au@SiO_2 NPs.

The measured fluorescence lifetime is very sensitive to the concentration of the silica nanoparticles due to the intermolecular quenching of the excited state, which will decrease for both multiple-molecule adsorbed on a single particle at low colloidal concentration and intermolecular quenching caused by LH2 adsorbed on a neighboring nanoparticle owing to agglomeration at high colloidal concentration. Thus, the longest lifetime, indicating the lifetime of a single LH2 complex adsorbed on a single nanoparticle in a nonagglomerated state, was found within the colloidal concentration region. Explicitly, the concentration of LH2 was fixed at $OD_{850nm} \approx 1.0$ cm^{-1}, and the colloidal concentration was varied from 0.05 to 10 g/L. For interaction between adjacent LH2s adsorbed at a single nonagglomerated nanoparticle, two extreme cases with large and small particle size respectively can be expected. For a

dx.doi.org/10.1021/jp211841a | J. Phys. Chem. C 2012, 116, 6993−6999

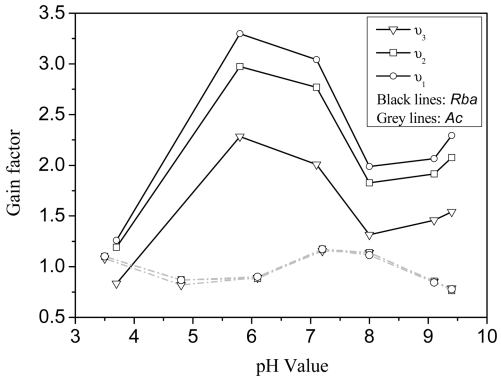

Figure 4. pH-dependent gain factors for three different vibrational modes of carotenoid molecules within LH2 from *Rba. sphaeroides* (solid lines) and *Rps. acidophila*, respectively (dash−dot lines). The lines are used for the guide of view.

nanoparticle with a large size, i.e., the diameter of the particle is much larger than that of LH2, there would be a great possibility of two or more neighboring LH2s being in close contact on the nanoparticle surface at an excess of LH2. For a small nanoparticle with its diameter being smaller than that of the LH2, in this case, at least two LH2 can be stacked on the nanoparticle like a sandwich also at an excess of LH2. For both the cases, the lifetime of LH2 would decrease due to the excited-state annihilation between the neighboring LH2s.[17] Figure 5 presents the normalized

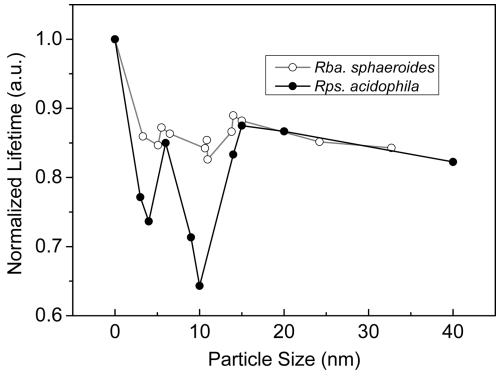

Figure 5. Normalized excited-state lifetime of LH2 from *Rba. sphaeroides* and *Rps. acidophila* respectively against particle size when adsorbed onto silica NPs.

excited-state lifetime measured for LH2 from *Rba. sphaeroides* and *Rps. acidophila*, respectively. The lifetime of free LH2 in solution measured for the former is 1.28 and 1.20 ns for the latter.

Asymmetrical Location of Car Molecules and B850 BChl Ring Inside the LH2. X-ray crystal structure of LH2 from the photosynthetic bacteria (*Rps. acidophila*)[18] shows that it consists of 9 α/β-apoprotein dimers associated to form a nonameric cylindrical structure. Each α/β-heterodimer binds noncovalently three BChl molecules, with two of which (dimer) of strong interaction form an aggregated BChl ring termed as B850 and the monomeric one as B800. The B850 ring is located closer to the periplasmic side (C-terminal) while the B800 ring is close to the cytoplasmic side (N-terminal) of the complex. Each α/β-heterodimer also contains a single Car molecule called rhodopsin-glucoside, the glucosyl group is located in a hydrophobic pocket on the cytoplasmic side of the complex, while the Car polyene chain runs through the macrocycle of the B800, progresses into the neighboring α/β-heterodimer, and passes over the face of the BChl 850. The long axis of the Car runs parallel to the transmembrane helices of the α- and β-polypeptide. The conformation of Car molecule is twisted adopting a semihelical structure viewed along its long axis.[13] The end of the Car polyene shows a distance about 0.8 nm from the periplasmic side, giving an asymmetrical location with respect to the two end surfaces as illustrated in Figure 6. For

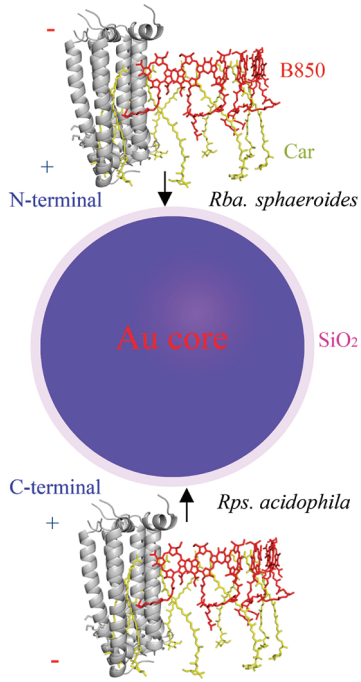

Figure 6. Schematic diagrams showing asymmetric location of carotenoid molecules and B850 BChl ring inside LH2 and interfacial binding to negatively charged Au@SiO_2 NPs with different sides. Only one-third of the helices are displayed for clarity.

LH2 from *Rba. sphaeroides*, although its crystal structure has not been available yet, the electron micrography (EM)[19] and atomic force micrography (AFM)[20] images of its 2D crystal show that it also exists as a nonamer. It contains sphaeroidene as the only carotenoid molecule when grown photosynthetically under anaerobiosis.[21] By use of surface-enhanced resonance Raman scattering (SERRS), it has been demonstrated that the sphaeroidene in LH2 from *Rba. sphaeroides* is preferentially located near the membrane's cytoplamic side,[15,22] same as those in LH2 from *Rps. acidophilia*.[18,23] Therefore, it is expected that the SHINERS of Car would have a different Raman gain when LH2 binds onto Au@SiO_2 NP with one of its two different end faces. We have also shown by small-angle X-ray scattering (SAXS) experiments that both the LH2s from the different strains have an elliptical topological structure in solution,[24,25] indicating that the protein frames are flexible and the nanoparticle-induced protein deformation may lead to a detectable change in the excited-state lifetime of LH2.

Surface Electrostatic Property of LH2. All 18 C-termini of the α- and β-polypeptides are located at the periplasmic side and the 18 N-termini at the cytoplasmic side. However, for LH2 from *Rps. acidophila*, the most positively charged part of LH2 corresponds to the C-terminal end where there are 18 positively charged lysine (K), two associate to each α-polypeptide.

dx.doi.org/10.1021/jp211841a | J. Phys. Chem. C 2012, 116, 6993−6999

Table 1. Comparison of the Amino Acid Sequences for LH2 from *Rps. acidophila* and *Rba. sphaeroides*

Rps. acidophila α-peptide	MNQGKIWTVVNPAIGIPALLGSVTVIAILVHLAILSHTTWFPAYWQGGVKKAA
Rba. sphaeroides α-peptide	MTNGKIWLVVKPTVGVPLFLSAAVIASVVIHAAVLTTTTWLPAYYQGSAAVAAE
Rps. acidophila β-peptide	ATLTAEQSEELHKYVIDGTRVFLGLALVAHFLAFSATPWLH
Rba. sphaeroides β-peptide	MTDDLNKVWPSGLTVAEAEEVHKQLILGTRVFGGMALIAHFLAAAATPWLG

The N-terminal regions are negatively charged because of the presence of 27 glutamic residues (E) in β-polypeptide. Molecular simulation illustrating the charge distribution of LH2 also reveals that C-termini are positively charged and N-termini are negatively charged.[26] Bopp et al. have immobilized LH2 from *Rps. acidophila* to a negatively charged mica surface and conducted a single LH2 complex fluorescence study excited by polarized light. Their result shows that the fluorescence polarization change for B800 ring is more significant than that of B850, indicating that the B850 ring is closest to the mica surface. The fact suggests that the periplasmic side of LH2 is positively charged. Therefore we expect that LH2 from *Rps. acidophila* would bind onto the Au@SiO_2 NP with its positively charged C-termini, i.e., with C-termini facing the NP and N-termini exposing to the solution. In this configuration, the Car molecule is away from the Au core and would have a smaller surface-enhanced Raman gain.

For LH2 from *Rba. sphaeroides*, its amino acid sequence is different from that of *Rps. acidophila* as shown in Table 1,[20] where the amino acid with positively charged side groups are marked in blue, while those of negatively charged are marked in red. The sequences forming trans-membrane helices for *Rps. acidophila* are underlined. Apparently in the C-terminal where two positively charged K in *Rps. acidophila* are replaced by two neutral amino acids, i.e., aniline (A) and valine (V), respectively, and an additional negatively charged E being as the end residue of the C-termini. Consequently periplasmic side (C-terminal) of LH2 from *Rba. sphaeroides* would be negatively charged. For the cytoplasmic side (N-terminal), a significant difference from that of *Rps. acidophila* is that the amino acid sequence of β-polypeptide becomes much longer, which may shift the three E further into the transmembrane helices and their electric charges would have less effect on the cytoplasmic side. Thus, only the charges on those more exposed amino acids are considered. There is one K in both the α- and β-polypeptide, and two aspartic acid (D) in the β-polypeptide. The isoelectric point for K and D is estimated to be 7.2, therefore the 18 end residue M (methionine) with a pK = 9.28[27] would make the cytoplasmic side (N-terminal) positively charged. As a result, the electric polarity with respect to the two end faces of LH2 from *Rba. sphaeroide* is just opposite to that from *Rps. acidophila*. It is expected that the cytoplasmic side of LH2 from *Rba. sphaeroides* would face the negatively charged silica NPs when self-assembling occurs. In this configuration the Car molecule would be closest to the Au NP surface and has a larger surface-enhanced Raman gain. The electrostatic property of these two different LH2s and their corresponding possible binding to the core−shell Au NP are displayed schematically in Figure 6.

Binding Side of the LH2 Protein Complex onto Au@SiO_2 NPs Revealed by Surface-Enhanced Raman Gains of Carotenoid Molecules. Both the surface-enhanced Raman spectra of Car molecules in LH2 from *Rba. sphaeroides* at resonant (Figure 3a) and nonresonant excitation (Figure 3b) show an unambiguous surface enhanced effect by the encapsulated Au core (In Figure 3b, the maximum gain factor is around 1.2. Those less than unity can be caused by the pH effect since the RR signal of free LH2 at pH of 8.0 is used for scaling reference). The fact suggests that the LH2 complexes have been assembled onto the silica shell. Furthermore, the three different vibrational modes of Car (Figure 3a and b) have a varied gain showing a typical feature of surface plasmon enhanced Raman scattering.[15] In principle, a comparison of SERRS and RR spectral peak intensity ratios (or the relative gain factor in SERRS) would reflect the orientational information regarding the molecules located at the surface of the Au core (e.g., proximity of structural moiety toward the metal surface). This is not the case with carotenoids. The modes observed in carotenoid spectra are delocalized throughout the conjugated chain. Hence, the relative intensity of a particular band in the SERRS spectrum cannot be ascribed to the proximity of the specific functional group or region of the carotenoid molecules to the Au surface. Some relative intensity difference are observed for υ_1 and υ_2, where a significant enhancement in υ_1 occurs relative to υ_2 in the SERRS. These changes may reflect a perturbation of the excited state of the carotenoid, resulting from its interaction with the Au plasmon band, this interaction could change the contribution of the individual vibronic states to the resonance enhancement, leading to the different gain factors for the different vibrational modes.[15] However, the surface-enhanced Raman spectrum at nonresonant excitation (Figure 3c) shows a significant larger gain factor for υ_3 over those of υ_1 and υ_2, which indicates that the methyl group of sphaeroidene is closest to the silica shell, in accordance with the fact that sphaeroidene has methyl groups at its two ends.

The electrostatic property of the two end surfaces of LH2 from *Rps. acidophila* is opposite to that from *Rba. sphaeroides*, which indicates that the former would bind to the silica shell with its periplasmic side where the Car molecule rhodopsin-glucoside is away from the shell surface at least by 0.8 nm. Even though the SiO_2 shell on Au core used to enhance the Raman scattering signal for LH2 from *Rps. acidophila* is slightly thinner than that used for LH2 from *Rba. sphaeroides*, the observed surface-enhance Raman gain factors for the former are smaller than those of the latter by a factor around 2 at their optimal binding. This observed phenomenon can be interpreted by the fact that Car is asymmetrically located inside the LH2 complex, and the interfacial assembling of LH2 onto Au@SiO_2 NPs occurring at different sides for LH2 from *Rba. sphaeroides* and *Rps. acidophila*.

Binding Side of the LH2 onto Au@SiO_2 NPs Confirmed by Excited-State Lifetime of the B850 BChl Ring. Structure-based spectroscopic properties of LH2 have been intensively investigated.[28−31] We have demonstrated before that when LH2 is adsorbed onto NPs, the latter would induce a structural deformation on LH2 protein frame, leading to a destruction of the circular symmetry of B850 ring giving

dx.doi.org/10.1021/jp211841a | J. Phys. Chem. C 2012, 116, 6993−6999

rise to a decrease in the excited-state lifetime.[9] This can be understood in terms of the oscillator strength of the lowest excited state, which is an optical transition forbidden state for a perfect ring corresponding to a zero oscillator strength, having a nontrival value owing to the random disorder in BChl interpair interaction[32] and a correlated disorder given by the structural deformation. Like Car molecules, B850 ring is also asymmetrically located inside the LH2 being closest to the periplasmic side. Therefore it is expected that when the B850 ring gets the closer to the silica curved surface, the stronger the distortion that the B850 ring would have. As shown in Figure 5, the excited-state lifetime of B850 of LH2 from *Rps. acidophila* undergoes a more drastic decrease when adsorbed silica NPs with a particle size smaller than 15 nm. Such a "W" shaped curves can be interpreted by Coloumbic interactions between the charged silica with the ends of two concentric cylinders consisting of α- and (outer ring) β-polypeptides (inner ring) respectively, both would lead to a deformation of B850 ring hence a change in the observed lifetime. The two maxima in the plot of lifetime versus the particle size indicate that the strongest interaction occurs when the particle size is close to that of the inner or outer polypeptide ring respectively. A detailed physical account of NP-induced LH2 protein deformation will be given later. Obviously, Figure 5 indicates that the nanoparticle-induced structural deformation of B850 ring is much larger in LH2 from *Rps. acidophila* than that from *Rba. sphaeriodes*, suggesting B850 ring in LH2 from *Rps. acidophila* is closer to the silica sphere than that of *Rba. sphaeriodes*. The fact strongly supports that LH2s from *Rps. acidophila* and *Rba. sphaeriodes* bind to the silica shell with different sides, i.e., the former with periplasmic side while the latter with cytoplasmic side (see Figure 6).

CONCLUSIONS

We have developed an efficient method for detecting the interfacial binding between the proteins and silica NPs by using a recently invented technique known as SHINERS. Basically our method is a modified surface-enhanced Raman scattering technique, utilizing the chemical properties of the shell to bind proteins and the physical property of core to produce enhanced electromagnetic field and enhanced Raman signal. We demonstrated the feasibility of this method by probing the protein orientation at the interface for two different bacterial photosynthetic light-harvesting complexes LH2s from *Rba. sphaeroides* and *Rps. acidophila* respectively, using Car molecules as the inherit reporters of Raman scattering. We find that these two different LH2 bind onto the silica shell with different orientation, i.e., for LH2 from *Rba. sphaeroides*, the positively charged cytoplasmic side (N-terminal) faces the negatively charged silica surface and with Car molecules being closest to the interface thus having a larger Raman gain. For LH2 from *Rps. acidophila*, the positively charged side is periplasmic side (C-terminal) which binds onto the silica shell with Car molecules being away from the interface, having a relatively smaller Raman gain factor. This conclusion is further supported by the significant difference in the measured change in the excited-state lifetime of the B850 BChl ring of the LH2s from the two different strains when adsorbed on silica nanoparticles, where the lifetime of B850 ring asymmetrically located inside LH2 is an intrinsic reporter for the extent of ring deformation induced by the interfacial interaction.

AUTHOR INFORMATION

Corresponding Author

*Phone: +86-10-82648118. Fax: +86-10-82648118. E-mail: yxweng@aphy.iphy.ac.cn.

Notes

The authors declare no competing financial interest.

ACKNOWLEDGMENTS

This work is supported by the Natural Science Foundation of China (grant 20925313), National Basic Research Program of China (grant 2009CB930700), and Chinese Academy of Sciences Innovation Program (KJCX2-YW-W25). Dr. Manping Ye is kindly acknowledged for the fluorescence lifetime measurement of LH2 from *Rps. acidophila*.

REFERENCES

(1) Aubin-Tam, M. E.; Hamad-Schifferli, K. *Biomed. Mater.* **2008**, *3*, 034001.
(2) Xu, Z.; Liu, X. W.; Ma, Y. S.; Gao, H. W. *Environ. Sci. Poll. Res.* **2010**, *17*, 798−806.
(3) Nabiev, I.; Rakovich, A.; Sukhanova, A.; Lukashev, E.; Zagidullin, V.; Pachenko, V.; Rakovich, Y. P.; Donegan, J. F.; Rubin, A. B.; Govorov, A. O. *Angew. Chem. Intern. Ed.* **2010**, *49*, 7217−7221.
(4) Oda, I.; Hirata, K.; Watanabe, S.; Shibata, Y.; Kajino, T.; Fukushima, Y.; Iwai, S.; Itoh, S. *J. Phys. Chem. B* **2006**, *110*, 1114−1120.
(5) Noji, T.; Kamidaki, C.; Kawakami, K.; Shen, J. R.; Kajino, T.; Fukushima, Y.; Sekitoh, T.; Itoh, S. *Langmuir* **2011**, 3690−3700.
(6) Höök, F.; Vörös, J.; Rodahl, M.; Kurrat, R.; Böni, P.; Ramsden, J.; Textor, M.; Spencer, N.; Tengvall, P.; Gold, J. *Colloid. Surf. B: Biointerf* **2002**, *24*, 155−170.
(7) Su, T.; Lu, J.; Thomas, R.; Cui, Z.; Penfold, J. *Langmuir* **1998**, *14*, 438−445.
(8) Li, J. F.; Huang, Y. F.; Ding, Y.; Yang, Z. L.; Li, S. B.; Zhou, X. S.; Fan, F. R.; Zhang, W.; Zhou, Z. Y.; Wu, D. Y.; Ren, B.; Wang, Z. L.; Tian, Z. Q. *Nature* **2010**, *464*, 392−395.
(9) Chen, X. H.; Zhang, L.; Weng, Y. X.; Du, L. C.; Ye, M. P.; Yang, G. Z.; Fujii, R.; Rondonuwu, F. S.; Koyama, Y.; Wu, Y. S.; Zhang, J. P. *Biophys. J.* **2005**, *88*, 4262−4273.
(10) Bose, S. *Bacterial Photosynthesis* **1963**, 501−510.
(11) Caruso, F.; Lichtenfeld, H.; Giersig, M.; Möhwald, H. *J. Am. Chem. Soc.* **1998**, *120*, 8523−8524.
(12) Yamada, K.; Yoshii, S.; Kumagai, S.; Fujiwara, I.; Nishio, K.; Okuda, M.; Matsukawa, N.; Yamashita, I. *Jpn. J. App. Phys., Part 1* **2006**, *45*, 4259.
(13) Gall, A.; Gardiner, A. T.; Cogdell, R. J.; Robert, B. *FEBS Lett.* **2006**, *580*, 3841−3844.
(14) Sashima, T.; Koyama, Y.; Yamada, T.; Hashimoto, H. *J. Phys. Chem. B* **2000**, *104*, 5011−5019.
(15) Picorel, R.; Lu, T.; Holt, R. E.; Cotton, T. M.; Seibert, M. *Biochemistry* **1990**, *29*, 707−712.
(16) Moskovits, M.; Suh, J. *J. Phys. Chem. B* **1984**, *88*, 5526−5530.
(17) Pflock, T. J.; Oellerich, S.; Krapf, L.; Southall, J.; Cogdell, R. J; Ullmann, G. M.; Kohler, J. *J. Phys. Chem. B* **2011**, *115*, 8821−8831.
(18) McDermott, G.; Prince, S. M.; Freer, A. A.; Hawthornthwaite-Lawless, A. M.; Papiz, M. Z; Cogdell, R. J.; Isaacs, N. W. *Nature* **1995**, *374*, 517−521.
(19) Walz, T.; Jamieson, S. J.; Bowers, C. M.; Bullough, P. A.; Hunter, C. N. *J. Mol. Biol.* **1998**, *282*, 833−845.
(20) Scheuring, S. *J. Bio. Chem.* **2003**, *279* (5), 3620−3626.
(21) Chumanov, G.; Picorel, R.; Zarate, I. O.; Cotton, T. M.; Seibert, M. *Photochem. Photobio.* **2000**, *71*, 589−595.
(22) Picorel, R.; Holt, R.; Cotton, T.; Seibert, M. *J. Bio. Chem.* **1988**, *263*, 4374.
(23) Koepke, J.; Hu, X.; Muenke, C.; Schulten, K.; Michel, H. *Structure* **1996**, *4*, 581−597.
(24) Hong, X.; Weng, Y. X.; Li, M. *Biophys. J.* **2004**, *86*, 1082−1088.

(25) Du, L. C.; Weng, Y. X.; Hong, X. G.; Xian, D. C.; Katsumi, K. *Chin. Phys. Lett.* **2006**, *23*, 1861−1863.
(26) Chandler, D. E.; Gumbart, J.; Stack, J. D.; Chipot, C.; Schulten, K. *Biophys. J.* **2009**, *97*, 2978−2984.
(27) Doolittle, R. F. Database of nonredundant proteins, In *Prediction of protein structure and the principles of protein conformation*; Fasman, G. D., Ed.; Springer: New York, 1989.
(28) Cogdell, R. J.; Gall, A.; Köhler, J. *Q. Rev. Biophys.* **2006**, *39*, 227−324.
(29) Sundström, V.; Pullerits, T.; van Grondelle, R. *J. Phys. Chem. B* **1999**, *103*, 2327−2346.
(30) van Grondelle, R.; Novoderezhkin, V. I. *Phys. Chem. Chem. Phys.* **2006**, *8*, 793−807.
(31) Novoderezhkin, V. I.; van Grondelle, R. *Phys. Chem. Chem. Phys.* **2010**, *12*, 7352−7365.
(32) Monshouwer, R.; Abrahamsson, M.; van Mourik, F.; van Grondelle, R. *J. Phys. Chem. B* **1997**, *101*, 7241−7248.